Wetting transitions for the Ar-CO_2 interface: Modified-hypernetted-chain and density-functional-theory results

E. Bruno and C. Caccamo
Istituto di Fisica Teorica, Universitá di Messina, Messina, Italy

P. Tarazona
Departamento de Fisica del Estado Solido and Instituto de Fisica del Estado Solido, Universidad Autonoma, Cantoblanco, Madrid 28049, Spain

(Received 4 August 1986)

A model of fluid-argon—solid-CO_2 interface is investigated by means of density-functional (DF) -theory and modified-hypernetted-chain (MHNC) calculations. Both theoretical approaches predict complete wetting of the CO_2 wall from the bulk Ar vapor when this approaches the coexistence region. At a bulk vapor density $n_B\sigma^3=0.08$ and for an assigned wall-fluid coupling strength, the DF and MHNC estimates of the temperature for which complete wetting occurs are very close to each other ($T^*\simeq 1.16$), and to the coexistence temperature of the homogeneous bulk phase obtained through independent DF and MHNC calculations. The DF results also show the existence of a prewetting transition, very close to the coexistence line, and of a "surface spinodal line," that is a set of points near and inside the coexistence region, at which transverse correlations in the fluid near the wall diverge, while the adsorption or coverage remains finite. The MHNC does not have convergent solutions in regions too close to coexistence so that it is hard to detect the very short prewetting line; however, the extrapolated behavior of the transverse correlations and coverage, which both show a diverging trend on approaching a well-defined temperature, and of the density profile whose features, far from the wall, faster and faster herald in the approach to coexistence, all point to the occurrence of complete wetting. Moreover, in agreement with DF results, transverse correlations also show a diverging trend inside the coexistence region while the coverage remains finite, thus confirming the existence of a surface spinodal line.

I. INTRODUCTION

The occurrence of complete wetting at a model fluid-argon—solid-CO_2 interface has been much debated in the recent literature on inhomogeneous fluids.[1–11] The controversy stems essentially from the fact that density-functional theories[2–7] predict complete wetting for the above system, whereas approximate integral equations for the pair-correlation function,[8,9] and also specific computer simulation,[9] do not.

However, the capability of certain integral equations to predict wetting has been questioned recently,[12] and lattice-gas calculations,[13] as well as other computer-simulation results[14] and direct experimental evidence,[15] are available for systems very similar to the Ar-CO_2 interface, where complete wetting is seen to occur.

One line of investigation of this problem, different from those hitherto cited, is constituted by modified-hypernetted-chain (MHNC) calculations,[16–18] which we have preliminarily reported in a recent paper,[19] together with some new density-functional (DF) -theory results. We found that the occurrence of wetting transitions at the Ar-CO_2 interface is coherently indicated by the behavior of different physical quantities, and supported by a close agreement between the two different sets of calculations.

It is the purpose of this paper to give a full account of the results previously reported and of their physical implications in the context of a detailed discussion of both the MHNC and the density-functional approach, as applied to the present system.

One basic point of our preceding work was the use of the concept of "nonlocality" in the procedure which models the properties of an inhomogeneous fluid in terms of those of a locally homogeneous one. The idea of nonlocality is not a new one in the context of the literature on inhomogeneous fluids. Various authors have in the past used a nonlocal ansatz for the one-particle density,[6,20,21] and recently this kind of approach has been given a more rigorous foundation. In particular, it has been shown that some of the previous approximations in the application of the density-functional formalism actually correspond to keeping the lowest-order terms in a density-functional expansion of the Helmholtz free energy.[7,22]

The density-functional results we report here hinge on these last developments in that they are obtained by keeping higher-order terms of that expansion than previously done.

As far as the MHNC is concerned, the inhomogeneous bridge function $E(\mathbf{r},\mathbf{r}')$ is constructed from its homogeneous counterpart, by using a nonlocal ansatz for $n_c(\mathbf{r})$ (Ref. 19). We are not aware of other similar calculations for $E(\mathbf{r},\mathbf{r}')$. Moreover, it is a distinctive feature of these MHNC calculations to be very extensive, in the sense that we perform an exploration of the dependence of the results on the truncation and discretization procedure of the direct and reciprocal space variables. It appears that this

last aspect can become crucial in order for the onset of the wetting transition to be observable or not.

The MHNC and the density-functional theory are expected to yield complementary physical information. In fact, the density-functional approach permits a detailed investigation of the thermodynamic region where the wetting transition is expected to occur. By contrast, the MHNC has no convergent solution when one appoaches too closely the transition region, due to the onset of long-range correlations in the fluid, but it embodies, e.g., direct information on the inhomogeneous two-particle distribution functions, which are not trivially obtainable within the density-functional-theory framework.

The comparison between the two theories is built up by first ensuring that they describe the bulk homogeneous fluid on a comparable level of accuracy. To this aim we specifically investigate the phase diagram of bulk Ar, modeled as a Lennard-Jones (LJ) 12-6 fluid, by the two methods.

This paper is arranged as follows. In Sec. II we cast the basic MHNC equations and describe the solution procedure; Sec. III reports the MHNC results; Sec. IV describes the density-functional approach, whose results are presented in Sec. V; a concluding discussion is given in Sec. VI.

II. MHNC BASIC EQUATIONS AND SOLUTION PROCEDURE

We consider a fluid consisting of molecules which interact through the LJ 12-6 potential

$$\phi_{LJ}(r)=4\varepsilon\left[\left[\frac{\sigma}{r}\right]^{12}-\left[\frac{\sigma}{r}\right]^{6}\right] \tag{1a}$$

with the parameters ε and σ appropriate to represent Ar ($\varepsilon/k_B=119.73$ K and $\sigma=3.405$ Å), and a substrate which is assumed to be a flat impenetrable wall of infinite extent in the x and y directions, and generating the (integrated) LJ 9-3 potential

$$V_{\rm ext}(z)=\alpha 4\pi\varepsilon_w n_w\sigma_w^3\left[\frac{1}{45}\left[\frac{\sigma_w}{z}\right]^9-\frac{1}{6}\left[\frac{\sigma_w}{z}\right]^3\right],\quad z>0$$
$$V_{\rm ext}(z)=\infty,\quad z\le 0 \tag{1b}$$

z being the distance from the wall. In (1b) α is an adjustable parameter which allows one to vary the strength of the substrate-fluid interaction. The other parameters are chosen in such a way to represent a solid CO_2 wall: $\varepsilon_w/k_B=153$ K, $\sigma_w=3.77$ Å, and $n_w\sigma_w^3=0.988$.[2]

The procedure of solution of the MHNC we follow has been described in detail elsewhere[17,18,23] and we discuss below only the manner in which the bridge function $E(\mathbf{r},\mathbf{r}')$ is modeled in terms of the hard-sphere bridge function.

We start from the first Born-Green-Yvon (BGY) equation for the inhomogeneous one-particle density $n(\mathbf{r})$,

$$\nabla[\ln n(\mathbf{r})+\beta V_{\rm ext}(\mathbf{r})]=\int d\mathbf{r}'c(\mathbf{r},\mathbf{r}')\nabla n(\mathbf{r}')\ , \tag{2}$$

and the Ornstein-Zernike equation

$$h(\mathbf{r},\mathbf{r}')-c(\mathbf{r},\mathbf{r}')=\int d\mathbf{r}''h(\mathbf{r},\mathbf{r}'')n(\mathbf{r}'')c(\mathbf{r}'',\mathbf{r}')\ , \tag{3}$$

where $h(\mathbf{r},\mathbf{r}')$ and $c(\mathbf{r},\mathbf{r}')$ are the total and direct inhomogeneous two-particle correlation functions, respectively. Note that, because of the planar symmetry of our system, one has $n(\mathbf{r})\to n(z)$, $c(\mathbf{r},\mathbf{r}')\to c(z,z',R)$, $h(\mathbf{r},\mathbf{r}')\to h(z,z',R)$, where $R=[(x-x')^2+(y-y')^2]^{1/2}$.

Equations (2) and (3) contain the three unknown functions $n(\mathbf{r})$, $h(\mathbf{r},\mathbf{r}')$, and $c(\mathbf{r},\mathbf{r}')$ and a closure can be obtained through the equation

$$h(\mathbf{r},\mathbf{r}')-c(\mathbf{r},\mathbf{r}')=\ln[1+h(\mathbf{r},\mathbf{r}')]+\beta\phi_{\rm LJ}(|\mathbf{r}-\mathbf{r}'|)-E(\mathbf{r},\mathbf{r}')\ , \tag{4}$$

which is an extension to the inhomogeneous case of a well-known result for homogeneous fluids obtained through cluster-expansion techniques.[24]

A functional form must be assumed for the unknown bridge function $E(\mathbf{r},\mathbf{r}')$. We set

$$E(\mathbf{r},\mathbf{r}')=E_{\rm HS}\left[|\mathbf{r}-\mathbf{r}'|;n_c\left[\frac{\mathbf{r}+\mathbf{r}'}{2}\right]\right]\ , \tag{5}$$

where

$$n_c(\mathbf{r})=\left[\frac{\pi d^3}{6}\right]^{-1}\int_s d\mathbf{r}''n(\mathbf{r}+\mathbf{r}'')\ . \tag{6}$$

We have so defined a coarse-grained local density obtained by averaging over a sphere which, according to (5), is centered halfway in between point $\mathbf{r}$ and $\mathbf{r}'$, with a temperature-dependent diameter d.[25] This last turns out to be almost equal to the LJ 12-6 diameter σ. In what follows σ will be taken as unit length. We report here for comparison the previously used prescription for $E(\mathbf{r},\mathbf{r}')$ (Refs. 17,18, and 23)

$$E(\mathbf{r},\mathbf{r}')=E_{\rm HS}(|\mathbf{r}-\mathbf{r}'|;\bar{n}=\tfrac{1}{2}[n(\mathbf{r})+n(\mathbf{r}')])\ . \tag{7}$$

Nonlocality effects are embodied in (6) through the determination of the effective density in $E_{\rm HS}(|\mathbf{r}-\mathbf{r}'|;n_c[(\mathbf{r}+\mathbf{r}')/2])$ through which we approximate $E(\mathbf{r},\mathbf{r}')$. The ansatz (6) is in the spirit of previous nonlocal calculations within the density-functional approach[6,7,22] and allows avoiding the feature that $n_c(\mathbf{r})$ can assume, near the wall, values higher than the maximum possible packing density.[23]

Equations (2)—(6) have been solved simultaneously by iteration. Some input functions $n(\mathbf{r})$ and $y(\mathbf{r},\mathbf{r}')=h(\mathbf{r},\mathbf{r}')-c(\mathbf{r},\mathbf{r}')$ are necessary in order to initialize the procedure. Then an isothermal or isochore path is explored, by slowly varying the density or the temperature, respectively, in order to get closer and closer to the coexistence line [known from independent bulk calculation (see below)]. The density profiles and the $y(\mathbf{r},\mathbf{r}')$ generated at each step are used as input for the next thermodynamic state.

Various meshes for the space variable z and R and for the wave vector Q, associated with the two-dimensional Fourier transform of the correlation functions with respect to R, are used.[17] These meshes have spacings $\Delta z,\Delta R,\Delta Q$. The distance from the wall $z_{\rm max}$ marks the boundary of the inhomogeneous fluid; beyond this point we impose the condition that the density of the fluid equals that of the bulk. 30—100 iterations are necessary

TABLE I. MHNC calculations at $n_B^*=0.06$, $T^*=k_BT/\varepsilon=1.17$ (ε is the minimum of the LJ potential well for Ar), $\alpha=1$ and different truncations for z, R, and Q and spacings Δz, ΔR, and ΔQ, under the use of the nonlocal ansatz (6). The used meshes are identified through the number in the first column. h_1 and h_2 are the heights of the first and second maximum in the density profile, respectively. All the quantities are in dimensionless units. Grid 5 is the same employed in Ref. 18.

	ΔR	R_{max}	Δz	z_{max}	ΔQ	Q_{max}	h_1	h_2	Γ	H_{max}
1	0.1	3.9	0.11	5.83	0.375	13.625	0.692	0.222	0.436	4.77
2	0.2	5.8	0.15	5.85	0.2	5.8	0.732	0.198	0.396	3.75
3	0.1	3.9	0.15	5.85	0.375	13.625	0.794	0.221	0.457	4.61
4	0.1	2.9	0.11	5.83	0.375	10.875	0.700	0.205	0.396	3.88
5	0.1	3.9	0.11	4.29	0.375	13.625	0.598	0.159	0.278	3.01
6	0.2	5.8	0.11	5.83	0.2	5.8	0.698	0.201	0.384	3.88
7	0.2	5.8	0.15	5.85	0.2	7.8	0.751	0.205	0.412	4.00
8	0.149	5.81	0.15	5.85	0.2	5.8	0.719	0.193	0.389	3.67
9	0.2	7.8	0.15	5.85	0.2	5.8	0.733	0.198	0.397	3.78
10	0.2	5.8	0.15	5.85	0.149	5.81	0.732	0.198	0.396	3.75
11	0.2	5.8	0.15	7.95	0.3	8.7	0.831	0.239	0.504	4.74

in order to get convergence, this last becoming slower the more closely the transition region is approached.

III. MHNC RESULTS

The quantities studied are the adsorption or coverage

$$\Gamma=\int_0^\infty dz[n(z)-n_B]\ , \tag{8}$$

where $n_B=n(z=\infty)$ is the bulk number density of particles of the fluid, and the transverse structure factor

$$H(z,Q)=1+\int_0^\infty dz' n(z')\int d\mathbf{R}\, e^{i\mathbf{Q}\cdot\mathbf{R}} h(z,z',R)\ .$$

In what follows we shall focus our attention on the maximum of $H(z,Q)$ at $z\simeq 3$ and $Q=0$. This maximum, first associated[23] with the growth of a new layer of adsorbate at the corresponding distance from the wall, has been shown by Evans and Tarazona[4,5] to be a signature of the approach to complete wetting of the system.

We report in Table I results for both Γ and H_{max}. As immediately appears, Γ and H_{max} depend on z_{max}, and actually increase, in a substantial manner, when z_{max} is increased. Note, in particular, the increase with respect to a grid equal to that already employed by Hillebrand and Nieminen.[18]

The effect of varying the grid spacings is a minor one. The same can be said for the effect of the nonlocal ansatz for the bridge function (as can be seen from Table II) with, however, the new feature, with respect to local calculations, that the convergence of the iterative procedure is more stable and faster when (6), instead of (7), is used; this will obviously be important when one is approaching wetting transition conditions (see below).

Despite the fact that we cannot exhibit results for Γ and H_{max} in a situation very close to complete wetting because, as discussed above, we fail to obtain solutions in that case, the available results can be fitted onto an interpretative framework which indicates that the wetting transition has to occur.

We start observing that, in the approach to complete wetting at constant temperature, one should have $\Gamma\sim|\mu-\mu_{coex}|^{-\beta_s}$, μ_{coex} being the chemical potential at coexistence for the saturated bulk vapor, and β_s some critical index. Now it has been shown that a surface compressibility sum rule holds for such a system,[12]

$$\int_0^\infty dz[n(z)H(z,Q=0)-\beta n_B^2 K_T]=\beta^{-1}\left[\frac{\partial\Gamma}{\partial\mu}\right]_T\ ,$$

K_T being the isothermal compressibility. It follows that $H_{max}\sim|\mu-\mu_{coex}|^{-\beta_s-1}$.

We now follow a different thermodynamical path by keeping the density fixed and reducing the temperature by starting with $T>T_{coex}$; we are thus approaching the coexistence line along an isochore from above. In this case one has $\Gamma\sim|T-T_{coex}|^{-\beta_s}$ and $H_{max}\sim|T-T_{coex}|^{-\beta_s-1}$. These results can be easily proved starting from the isothermal expression for Γ and H_{max}, before reported, and by using standard thermodynamic derivation techniques.

In our calculations we use finite meshes so that we actually reduce the range of action of the potential; now, as it has been shown in Ref. 4, for a short range potential $\beta_s=0$, and therefore we obtain $\Gamma\sim\ln|T-T_{coex}|$ and $H_{max}\sim|T-T_{coex}|^{-1}$.

Rather than selecting different isochores we study the

TABLE II. MHNC calculations for the same thermodynamical point as in Table I, with $\Delta R=0.2$, $R_{max}=5.8$, and $\Delta z=0.15$. L stands for the local ansatz (7) and NL for our nonlocal calculation with the ansatz (6).

	z_{max}	ΔQ	Q_{max}	h_1	h_2	Γ	H
L	7.95	0.3	8.7	0.907	0.249	0.545	4.44
NL	7.95	0.3	8.7	0.831	0.239	0.504	4.74
L	5.85	0.2	5.8	0.758	0.200	0.407	3.57
NL	5.85	0.2	5.8	0.732	0.198	0.396	3.73

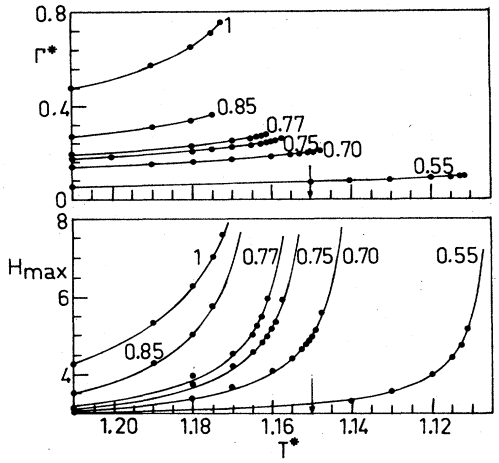

FIG. 1. Γ and H_{max} as a function of T^* at $n_B^*=0.08$, from MHNC. Mesh 2 (see Table I) is used here. Labels on the curves are α values. Solid circles correspond to computed points, solid lines to the fit law (see text). The arrows mark T_{coex} obtained from an independent MHNC bulk calculation.

behavior of H_{max} at fixed bulk density and as a function of α and temperature. Results for Γ and H_{max} according to this procedure are reported in Fig. 1.

At high α's H_{max} clearly shows a diverging trend, less visible in Γ, as could be expected on the basis of the above discussion. H_{max} is specifically calculated in a set of discrete points; in agreement with the discussion given above, these points can be fitted rather accurately with curves $C_1+C_2\,|\,T-T_{div}\,|$, C_1, C_2, and T_{div} being parameters of the fit. The extrapolated divergence temperature so obtained, $T_{div}(\alpha)$ is reported in Fig. 2.

It clearly appears that for $\alpha>0.72$, $T_{div}\simeq 1.15$; this temperature, quite remarkably, coincides with the MHNC coexistence temperature for the homogeneous bulk phase independently calculated, by using the same meshes as the inhomogeneous case. The bulk-phase diagram was calculated by using a method proposed by Ebner, Saam, and Stroud.[26] We show in Fig. 3 the bulk-phase diagram of

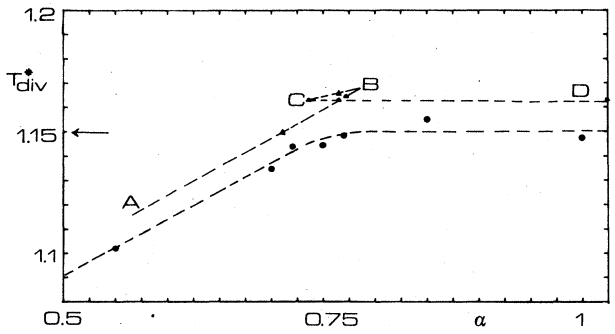

FIG. 2. T_{div} as a function of α, for $n_B^*=0.08$. Solid circles and triangles indicate, respectively, MHNC and density-functional results. Arrow: same source as Fig. 1. *AB* is the surface spinodal line, *BC* the prewetting line, and *CD* the complete wetting line, which is the straight line $T=T_{coex}$, from density-functional calculations.

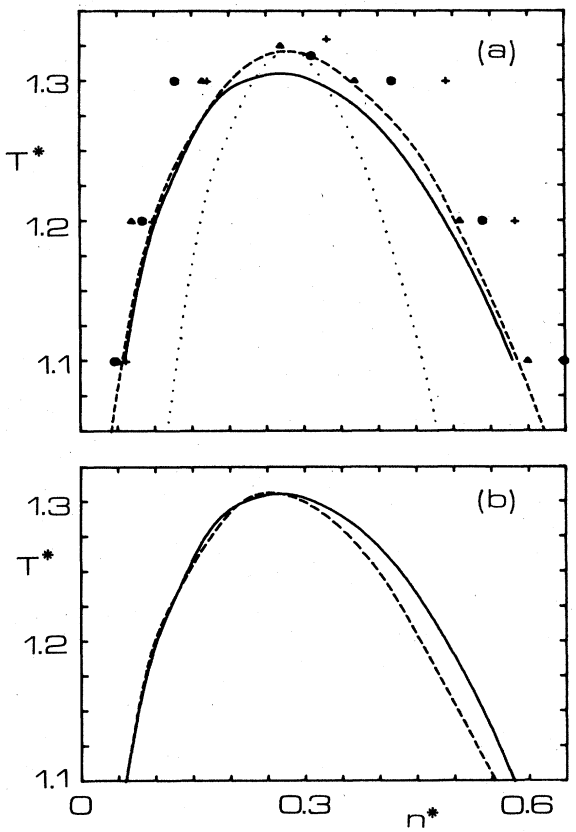

FIG. 3. Phase diagram for bulk Ar. In (a) the crosses are Monte Carlo results (Ref. 24); circles, Percus-Yevick calculations (Ref. 26); triangles, MHNC with a mesh of 1024 points; dashed line, MHNC with 64 points; solid line, MHNC with 32 points; dotted line, spinodal line with 64 points. In (b) the coexistence curve from a MHNC calculation with 32 points (solid line) is compared with the van der Waals one from Eqs. (13) and (14) (dashed line).

Ar according to different discretization procedures and truncations. The agreement with the phase diagram obtained by other authors is good and could be improved quite significantly through the use of more extended and finer grids. A calculation for the inhomogeneous system at this level of accurateness would, however, imply prohibitively large computing times and memory allocations, so that a reasonable compromise has to be found, on the basis of Fig. 3, between opposing necessities.

We now examine the functional dependence of Γ and H_{max} on the truncation with respect to z. Previous MHNC calculations performed by Hillebrand and Nieminen[18] seemed to exclude the possibility of finding complete wetting within the MHNC approach. We plot a set of isothermal calculations in Fig. 4; it appears that, when z_{max} is great enough, the coverage, instead of saturating in the approach to the coexistence line, tends to diverge. This behavior is even more clearly illustrated in Fig. 5 where we report, at fixed bulk density, various density profiles at different α's and temperatures. In this case increasing α corresponds to a decrease of the wetting temperature T_w; this explains the two different regimes for

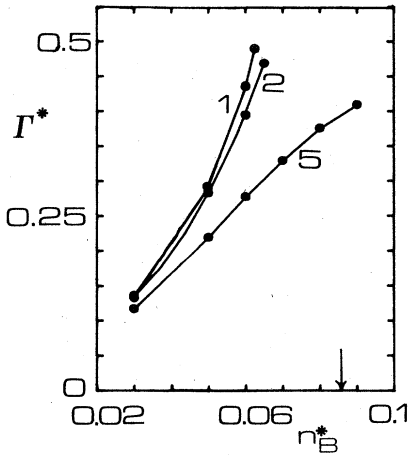

FIG. 4. Γ vs n_B at $\alpha=1$, along the isotherm $T^*=1.17$. Labels identify the meshes employed (see Table I). The arrow marks n_B at coexistence for the vapor. Note that, in curve 5 (the same choice of mesh as Ref. 18), Γ tends to saturate with increasing n_B.

$n(z)$ shown in the figure. At high α's small variations in the temperature toward the coexistence line result in a strong enhancement of the height of the second peak; however, the boundary condition $n(z)=n_B$ for $z>6$ evidently frustrates the possible growth of a plateau after the second peak.

The analysis of the three sets of results for Γ, $H_{\max}$, and $n(z)$ indicates that the system approaches complete wetting as $T^*\to 1.15$, although the theory is able to describe this phenomenon only up to its preliminaries.

As it appears from Fig. 1 divergences can occur in $H_{\max}$ also for low α's. This seems apparently to contrast with the possibility of identifying in a unique manner the temperature at which wetting occurs. However, one must observe that even if $H_{\max}$ is divergent, Γ is not and actually is almost independent from T. Moreover, the divergences in $H_{\max}$ occur now for $T<T_{\text{coex}}$, and therefore it is plausible that they have a different physical origin from those described above and associated with the occurrence of complete wetting. As we show in the following sections a close inspection of the results leads to the identification of a "surface spinodal line" whose physical features are consistent with the concept of "surface spinodal decomposition," previously introduced by Nakanishi and Pincus[27] within the framework of a Landau model of a fluid-wall interface.

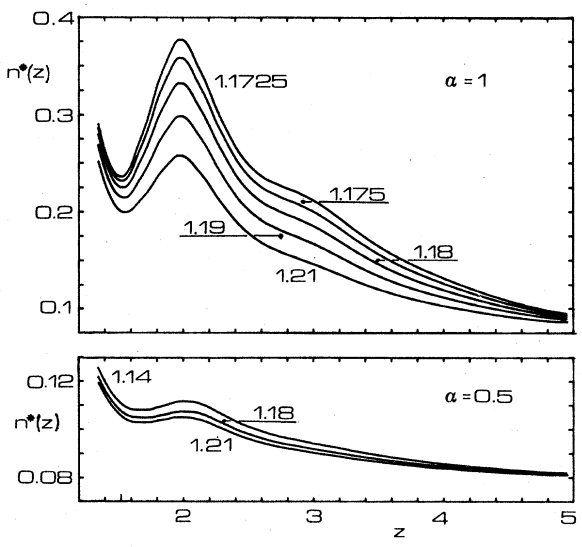

FIG. 5. Density profiles in the region $z>1.5$ (in σ units) for two cases of Fig. 1. Labels identify the temperatures.

IV. FREE-ENERGY DENSITY MODEL

Within the density-functional formalism, the density distribution $n(\mathbf{r})$ of a fluid in presence of an external potential $V_{\text{ext}}(\mathbf{r})$ may be obtained by minimizing the grand potential energy

$$\Omega[n(\mathbf{r})]=\mathcal{F}[n(\mathbf{r})]+\int d\mathbf{r}[V_{\text{ext}}(\mathbf{r})-\mu]n(\mathbf{r}) , \tag{9}$$

where μ is the chemical potential and $\mathcal{F}[n(\mathbf{r})]$ the intrinsic free-energy density functional,[28] which will depend on the internal interactions in the fluid. Here we consider $\mathcal{F}[n(\mathbf{r})]$ divided into two terms,

$$\mathcal{F}[n(\mathbf{r})]=\mathcal{F}_{\text{HS}}[n(\mathbf{r})] +\tfrac{1}{2}\int d\mathbf{r}\int d\mathbf{r}' n(\mathbf{r})n(\mathbf{r}')\phi_{\text{att}}(|\mathbf{r}-\mathbf{r}'|) , \tag{10}$$

where the first part gives the contribution to the free energy of the core repulsions, taken as hard-sphere interactions, and $\phi_{\text{att}}(r)$ is defined below. $\mathcal{F}_{\text{HS}}[n(\mathbf{r})]$ has sometimes been taken in the local-density approximation to study the wetting transition,[3–5] but here we include the nonlocal dependence, which produces the layering of the fluid near the wall, by taking[7]

$$\mathcal{F}_{\text{HS}}[n(\mathbf{r})]=\mathcal{F}_{\text{id}}[n(\mathbf{r})]+\int d\mathbf{r}\, n(\mathbf{r})\Delta\psi_{\text{HS}}(\bar{n}(\mathbf{r})) , \tag{11}$$

where $\mathcal{F}_{\text{id}}[n(\mathbf{r})]$ is the exact free energy of an ideal gas, $\Delta\psi_{\text{HS}}(n)$ is the excess over ideal gas of the free energy per particle at homogeneous density n, obtained from the Carnahan-Starling (CS) equation of state, and

$$\bar{n}(\mathbf{r})\equiv\int d\mathbf{r}\, n(\mathbf{r}')w(|\mathbf{r}-\mathbf{r}'|;\bar{n}(\mathbf{r})) \tag{12}$$

is an averaged density at which $\Delta\psi_{\text{HS}}$ is evaluated. $\bar{n}(\mathbf{r})$ has a nonlocal dependence on $n(\mathbf{r})$, through the density-dependent weight function $w(r,\bar{n})$. This weight function is fixed to reproduce the first term in the virial expansion for the direct correlation function.[7] It is interesting to note that the zeroth-order term of this expansion turns out to be a step-function weight, very similar to the one used in Eq. (6) to obtain the density n_c at which the bridge function is evaluated in the MHNC calculation.

The second term in (10) is the contribution to the free energy coming from the attractive interactions in a mean-field approximation, so that $\phi_{\text{att}}(r)$ has to be considered as an effective potential between the LJ particles.

For a homogeneous system, (10) gives the generalized van der Waals equation of state[3]

$$P=P_{\text{HS}}+\tfrac{1}{2}\hat{\phi}_0 n^2 \tag{13}$$

and

$$\mu=\mu_{\rm HS}+\hat{\phi}_0 n \ , \tag{14}$$

where $p_{\rm HS}$ and $\mu_{\rm HS}$ are the pressure and the chemical potential in the CS equation of state, and

$$\hat{\phi}_0 \equiv \int d\mathbf{r}\,\phi_{\rm att}(r)$$

is the volume integral of the effective attractive interactions. The critical temperature and density predicted by Eqs. (13) and (14) are

$$k_B T_C = -0.0901\hat{\phi}_0/d_{\rm HS}^3 \tag{15}$$

and

$$n_{\rm cr}=0.249/d_{\rm HS}^3 \ ,$$

$d_{\rm HS}$ being the hard-sphere diameter.

In order to compare the density-functional results with those of the MHNC calculation one would like to have the bulk-phase diagram of both calculations as similar as possible. On the other hand, for the wetting properties of the model it is important to keep the exact long-range behavior of the attractive tail, that is

$$\phi_{\rm att}(r)=\phi_{\rm LJ}(r)=-4\varepsilon(\sigma/r)^6 \quad \text{for } r\to\infty \ . \tag{16}$$

In previous works,[5,6] $\phi_{\rm att}(r)$ has been taken as the negative part of the full LJ potential. However the critical temperature obtained from (15), with this choice for $\phi_{\rm att}(r)$, is far too low compared with the integral-equation calculations and with Monte Carlo simulations. The reason is that $\phi_{\rm att}(r)$ in (10) should represent the real interaction, $\phi_{\rm LJ}(r)$, weighted by the pair correlation function $g(r)$, which has the strong first peak just about the minimum of $\phi_{\rm LJ}(r)$, enhancing in this way the role of the attractive interactions over what could be the result of a pure mean-field model, when $g(r)$ is assumed to be 1 for all r. In order to consider this effect, without losing the requirement (16) for the long-range behavior, we have here taken

$$\phi_{\rm att}(r)=4\varepsilon\left[\lambda\left[\frac{\sigma}{r}\right]^{12}-\left[\frac{\sigma}{r}\right]^{6}\right], \quad r\geq\lambda^{1/6}\sigma$$

$$=0, \quad r\leq\lambda^{1/6}\sigma \tag{17}$$

where ε and σ are the LJ parameters in (1) and λ is a free new parameter which modifies the short-range repulsion. For $\lambda=1$, (17) gives the negative part of the LJ potential, but if λ is less than 1, $\phi_{\rm att}(r)$ has a lower minimum. We have fixed λ in order to obtain exactly the same critical temperature as in the MHNC calculation, that is, $T^*=1.307$, which implies $\lambda=0.5926$, with a minimum for $\phi_{\rm att}(r)$ of -1.68ε which corresponds to an enhancement of about 70% over the original LJ. This is reasonable in order to describe the effect of the peak in $g(r)$ at intermediate density. The hard-sphere diameter is fixed to be σ. The bulk diagram obtained is compared in Fig. 3 with the results of the bulk MHNC. There is a reasonable overall agreement, between the two phase diagrams, which is better at gas densities than at liquid densities, and particularly good for reduced temperatures between 1.1 and 1.2, precisely in the range extensively explored in the MHNC calculations.

Once the functional model for $\mathcal{F}[n(\mathbf{r})]$ is specified, we carry on the calculations by solving the Euler-Lagrange integral equation obtained by the functional derivative of (9), with the external potential (1b). The procedure to obtain the solutions near the wetting transition has been explained in detail elsewhere.[5-6] First the liquid-vapor and the wall-liquid density profiles are obtained and used to generate the initial guess for the wall-vapor interface, with a given thickness for the wetting film. After a few iterations of the integral equation, $n(z)$ goes to the line of constrained minima of the grand potential energy at fixed coverage, near the complete wetting regime and, along this line of constrained minima, $\Omega[n(\mathbf{r})]$ is a very smooth function of the wetting-layer thickness. It follows that the iterative procedure becomes very inefficient to move $n(z)$ towards the absolute minimum of the functional. However, by starting with initial guesses with different wetting-layer thickness, one may obtain the function $\gamma(\Gamma)$, giving the surface tension (or grand potential surface excess) along the line of constrained minima. The equilibrium state corresponds to the absolute minimum of $\gamma(\Gamma)$, but one also gets information on metastable states (relative minima) and a good estimate of the surface spinodal line as corresponding to the saddle points in $\gamma(\Gamma)$. This allows us not only to locate the wetting and prewetting transitions, but also to associate the divergences in the transverse structure factor, obtained in the MHNC, with a surface spinodal line.

V. RESULTS FROM THE DENSITY-FUNCTIONAL CALCULATION

In order to compare with the MHNC results reported in Sec. III we have done calculations at fixed temperature and bulk density, with variable strength for the wall potential. This allows us to compare the wetting behavior of the system with exactly the same bulk variables, but in contact with different walls. The calculations presented here always correspond to a fixed vapor density $n_B^*=n_B\sigma^3=0.08$ which, according to (13) and (14) is at coexistence with a liquid of density $n_L^*=0.4878$, at $T^*=1.1618$. This temperature is slightly higher than the coexistence value for the same vapor density obtained in the MHNC calculation, which was $T^*=1.15$.

In Fig. 6(a) we present the results for the surface tension of the wall-vapor interface at bulk coexistence, along the fixed coverage constrained minima line, for several values of the wall-strength parameter α. For $\alpha=0.7$ there is a well-defined minimum at about $\Gamma^*=\Gamma\sigma^2=0.4$ separated by a barrier from a metastable state at $\Gamma\to\infty$, which corresponds to a macroscopic wetting film (notice that the figure actually represents the difference of the surface tension with the perfect wetting state). The curve $\gamma(\Gamma)$ describes, for this value of α, a partial wetting situation. This is still the same for $\alpha=0.72$, but now the difference between the surface tensions of the thin film and the macroscopic wetting layer is reduced. For about $\alpha=0.74$ both states have the same surface tension, but they are still separated by a barrier, so that this corre-

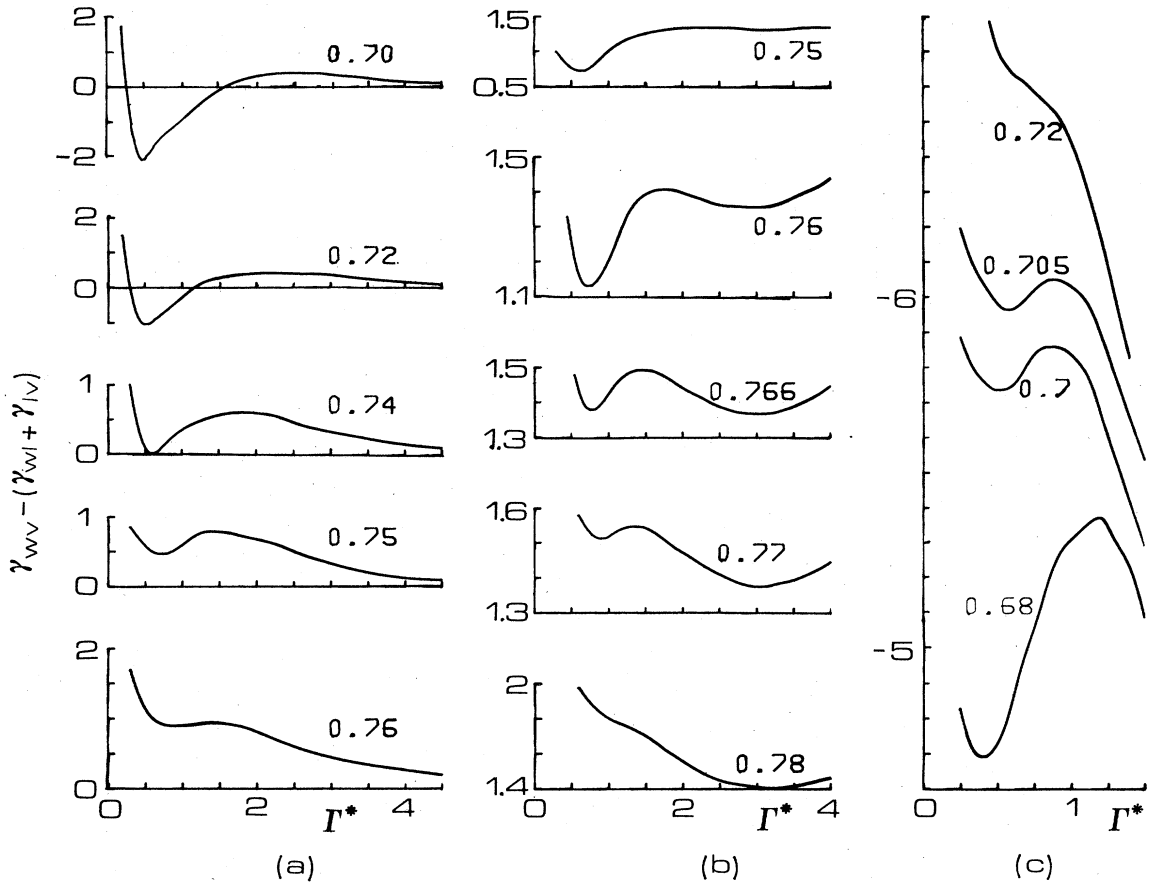

FIG. 6. The surface tension γ (plotted in units of $\varepsilon/\sigma^2\times10^{-2}$) vs the adsorption Γ, from density-functional calculation, at $n_B^*=0.08$ for different temperatures. Labels identify α values. (a) $T^*=1.1616$, the coexistence temperature; (b) $T^*=1.163$; (c) $T^*=1.15$.

sponds to the value of α at which the wetting transition occurs at $T^*=1.1618$. For $\alpha=0.75$ the thin film is still a local minimum, but now represents a metastable state against the true equilibrium profile given by $\Gamma\to\infty$. At $\alpha=0.76$ the local minimum is taken over the intermediate maximum, becoming a saddle point which represents the surface spinodal for the thin film, at this temperature.[27]

The surface spinodal marks, in the context of a mean-field calculation, the point at which the thin wetting layer becomes unstable, inside the coexistence region, with respect to growth; this situation will produce unbounded transverse correlations for a finite thickness of the wetting layer, as opposite to the approach to complete wetting, which last implies the divergence of the coverage and of the transverse correlations at the same point, i.e., at coexistence, for any $T>T_w$, but with different powers.

Figure 6(b) shows the curves $\gamma(\Gamma)$ for $T^*=1.163$, just 0.1% above the bulk coexistence, at fixed $n_B^*=0.08$, so that the liquid is not quite at coexistence with the bulk vapor. This changes the flat behavior of $\gamma(\Gamma)$ to a linear increase, proportional to the undersaturation of the bulk with respect to the coexisting vapor;[4] the minimum at $\Gamma\to\infty$ is then moved toward a finite Γ and the value of $\gamma(\Gamma)$ is increased, so that for $\alpha=0.76$ the absolute minimum is still a thin film of about $\Gamma^*=0.75$. At $\alpha=0.7663$ one finds two equivalent minima which correspond to the prewetting phase transition where a thin and a thick film coexist. Figure 7 shows the two coexisting profiles.

At larger α's the thick film is stable and just above $\alpha=0.77$ the thin one disappears with a surface spinodal point similar to that already described at bulk coexistence. At even larger temperatures the surface spinodal line will meet the prewetting line in the prewetting critical point.

Finally we present in Fig. 6(c) the results for $T^*=1.15$, below the coexisting temperature, so that the bulk vapor is metastable against the bulk liquid. $\gamma(\Gamma)$ has a negative slope at large Γ and the equilibrium configuration will always be the wall-liquid interface, rather than the wall-vapor interface. Moreover, for low α there is still a local minimum about $\Gamma^*=0.5$, which corresponds to the metastable wall-vapor interface, with a small adsorbed layer. As α is increased this layer increases until the local minimum disappears for $\alpha\simeq0.71$; this marks the position of the surface spinodal line inside the bulk coexistence curve.

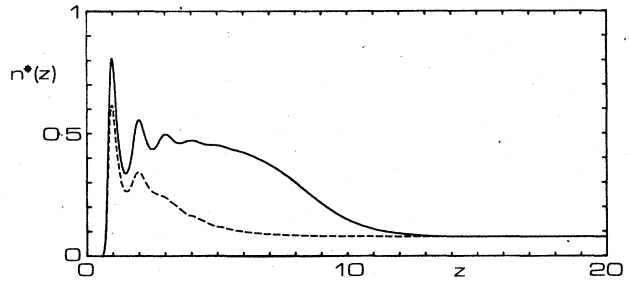

FIG. 7. Thick (solid line) and thin (dashed line) film at coexistence, along the prewetting line: density profiles for $n_B^*=0.08$, $T^*=1.163$, and $\alpha=0.7663$.

VI. DISCUSSION

The main results of our calculation are shown in the (α,T) diagram of Fig. 2. From the MHNC calculation we represent the temperature at which the transverse correlations diverge, as a function of the wall-strength parameter α. As we already commented in Sec. III, there are two regions characterized by a different behavior of the transverse structure factor: for $\alpha>0.75$ the divergence of $H(z,Q=0)$ occurs at a fixed temperature $T^*=1.15$, which is the bulk coexistence temperature, at the fixed value for the density of the bulk vapor, as obtained from an independent bulk MHNC calculation. This behavior may be associated with the growth of the wetting layer as the system approaches coexistence above the wetting temperature. For $\alpha<0.75$ the MHNC predicts the divergence of the transverse correlations at a lower temperature, dependent on α, inside the bulk coexistence curve. Moreover, the divergence of $H(z,Q=0)$ is not followed by a divergence of the coverage. All these features are explained by interpreting the divergence of the transverse correlation for $\alpha<0.75$ as a signature of the approach to the surface spinodal line described before.

The density-functional calculation does not give information on the surface correlations, but it gives the surface tension (or the grand potential surface excess) of the system, in each case. That makes it easier to identify the surface phase transitions and even the surface spinodals. The wetting and the prewetting transitions and the surface spinodal, as obtained by the density-functional approach, are presented in Fig. 2.

The agreement between the results of the MHNC and density-functional theories is remarkable, letting aside the slight difference between the bulk-coexistence temperature obtained in the two cases ($T^*_{\rm coex}=1.15$ and $T^*_{\rm coex}=1.1618$, respectively) that shifts the flat region of the curves from each other. The wetting values of α obtained (at the chosen n_B) are substantially the same ($\alpha\simeq0.75$), and even the slope of the surface spinodal in the (α,T) diagram is quite similar.

The prewetting transition, visible in the density-functional results and shown in Fig. 2 as a small loop very close to the wetting and coexistence temperatures, is clearly very hard to detect in the context of the MHNC theory,

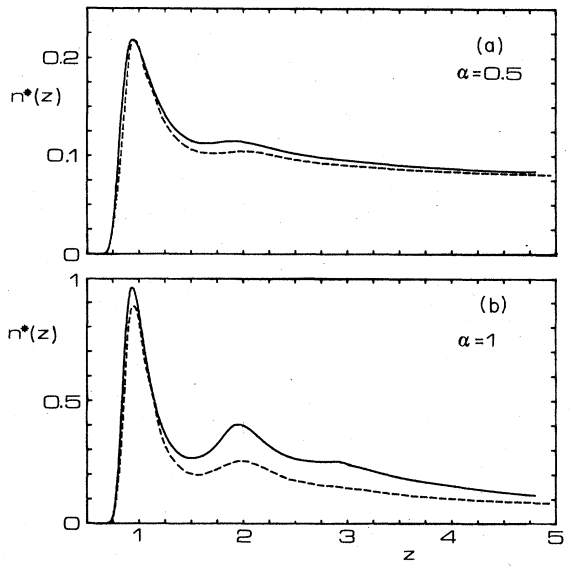

FIG. 8. Density profiles from MHNC (solid line) and density-functional (dashed line) calculation for $n_B^*=0.08$, $T^*=1.21$, and $\alpha=1$ (a) and 0.5 (b).

in which one has convergence problems when the correlation range becomes too large. Figure 7 illustrates more clearly the thin-thick film equilibrium and one can understand from the figure that, in order to see a similar pattern within the MHNC approach one should have very large values for $z_{\rm max}$ and the calculation would become prohibitively long and expensive.

However, in order to get a feeling for the agreement of the two theories, we have performed calculations in two situations not too close to the coexistence region. We have chosen $T^*=1.21$, and $\alpha=1$ and 0.5, respectively, and the same value for $z_{\rm max}$. The results for the density profile are shown in Fig. 8. As it is possible to see, there is a good overall agreement, particularly for the first peak height. At larger distances from the wall the agreement is not so good, mainly because the DF approach does not contain, at variance of the BGY equation, the condition of smooth joining of both the density and its derivative to the bulk values. In fact a jump would be visible in density-functional results if $z_{\rm max}$ were chosen too small.

The agreement of the predictions of the wetting properties, obtained from the study of the surface correlations in one case, and from surface thermodynamics in the other, according to two completely different theories as the MHNC and the density-functional model are, strongly supports the overall interpretation given here.

ACKNOWLEDGMENTS

This work has been supported by Gruppo Nazionale Struttura della Materia of Consiglio Nazionale delle Ricerche, Italy, and Centro Interuniversitario Struttura della Materia of Ministero Italiano della Pubblica Istruzione.

[1]J. W. Cahn, J. Chem. Phys. **66**, 3667 (1977).
[2]C. Ebner and W. F. Saam, Phys. Rev. Lett. **38**, 1486 (1977).
[3]D. E. Sullivan, Phys. Rev. B **20**, 3991 (1979).
[4]P. Tarazona and R. Evans, Mol. Phys. **48**, 799 (1983).
[5]R. Evans and P. Tarazona, Phys. Rev. A **28**, 1864 (1983).
[6]P. Tarazona and R. Evans, Mol. Phys. **52**, 847 (1984).
[7]P. Tarazona, Phys. Rev. A **31**, 2672 (1985).
[8]D. E. Sullivan and G. Stell, J. Chem. Phys. **69**, 5450 (1978); L. S. Smith and L. L. Lee, *ibid.* **71**, 4085 (1979).
[9]J. E. Lane, T. H. Spurling, B. C. Freasier, J. K. Perram, and E. R. Smith, Phys. Rev. A **20**, 2147 (1979).
[10]C. Teletzke, L. E. Schriven, and H. T. Davis, J. Colloid Interface Sci. **87**, 550 (1982).
[11]For a comprehensive updated review see also D. E. Sullivan and M. M. Telo da Gama, in *Fluid Interfacial Phenomena,* edited by C. A. Croxton (Wiley, London, 1985).
[12]R. Evans, P. Tarazona, and U. Marini Bettolo Marconi, Mol. Phys. **50**, 993 (1983).
[13]C. Ebner, Phys. Rev. A **22**, 2776 (1980); R. Pandit, M. Schick and M. Wortis, Phys. Rev. B **26**, 5112 (1982); M. P. Nightingale, W. F. Saam, and M. Schick, *ibid.* **30**, 3830 (1984) and references therein.
[14]C. Ebner, Phys. Rev. A **23**, 1925 (1981).
[15]R. Moldover and J. W. Cahn, Science **207**, 1073 (1980); D. W. Pohl and W. T. Goldburg, Phys. Rev. Lett. **48**, 1111 (1982); J. Suzanne, J. L. Seguin, M. Bienfait, and E. Lerner, *ibid.* **52**, 637 (1984).
[16]Y. Rosenfeld and N. W. Ashcroft, Phys. Rev. A **20**, 1208 (1979).
[17]R. M. Nieminen and N. W. Ashcroft, Phys. Rev. A **24**, 560 (1981).
[18]K. Hillebrand and R. M. Nieminen, Surf. Sci. **147**, 599 (1984).
[19]E. Bruno, C. Caccamo, and P. Tarazona, Phys. Rev. A **34**, 2513 (1986).
[20]J. Fisher and M. Methfessel, Phys. Rev. A **20**, 2836 (1980).
[21]B. Freasier and S. Nordholm, Mol. Phys. **54**, 33 (1985).
[22]W. A. Curtin and N. W. Ashcroft, Phys. Rev. A **32**, 2909 (1985).
[23]S. M. Foiles and N. W. Ashcroft, Phys. Rev. B **25**, 1366 (1982).
[24]J. P. Hansen and I. R. McDonald, *The Theory of Simple Liquids* (Academic, New York, 1976).
[25]The hard-core diameter d is chosen according to the same procedure of Foiles and Ashcroft (Ref. 23), $\phi_{LJ}(d)-\phi_{min}=3k_BT/2$, where ϕ_{min} is the minimum value of the two-body potential.
[26]C. Ebner, W. F. Saam, and D. Stoud, Phys. Rev. A **14**, 2264 (1976).
[27]H. Nakanishi and P. Pincus, J. Chem. Phys. **79**, 997 (1983).
[28]R. Evans, Adv. Phys. **28**, 143 (1979).